

# Spaceborne observations of the lidar ratio of marine aerosols

K. W. Dawson<sup>1</sup>, N. Meskhidze<sup>1</sup>, D. Josset<sup>2,#</sup>, and S. Gassó<sup>3</sup>

<sup>1</sup>Marine, Earth, and Atmospheric Science, North Carolina State University, Raleigh, NC, USA

<sup>2</sup>Science Systems and Applications, Inc/NASA Langley Research center

<sup>3</sup>GESTAR/Morgan State University, Goddard Space Flight Center, Greenbelt, Maryland

<sup>#</sup>Now at Naval Research Laboratory, Stennis Space Center,

*Correspondence to:* Nicholas Meskhidze (nmeskhidze@ncsu.edu)

## Abstract

Retrievals of aerosol optical depth (AOD) from the Cloud-Aerosol Lidar with Orthogonal Polarization (CALIOP) satellite sensor require the assumption of the extinction-to-backscatter ratio, also known as the lidar ratio. This paper evaluates a new method to calculate the lidar ratio of marine aerosols using two independent sources: the AOD from the Synergized Optical Depth of Aerosols (SODA) and the integrated attenuated backscatter from CALIOP. With this method, the particulate lidar ratio can be derived for individual CALIOP retrievals in single aerosol layer, cloud-free columns over the ocean. Global analyses are carried out using CALIOP level 2, 5km marine aerosol layer products and the collocated SODA nighttime data from December 2007 to November 2010. The global mean lidar ratio for marine aerosols was found to be 26 sr, roughly 30% higher than the current value prescribed by the CALIOP standard retrieval algorithm. Data analysis also showed considerable spatiotemporal variability in the calculated lidar ratio over the remote oceans. The calculated marine aerosol lidar ratio is found to vary with the mean ocean surface wind speed ( $U_{10}$ ). An increase in  $U_{10}$  reduces the mean lidar ratio for marine regions from  $32 \pm 17$  sr (for  $0 < U_{10} < 4 \text{ ms}^{-1}$ ) to  $22 \pm 7$  sr (for  $U_{10} > 15 \text{ ms}^{-1}$ ). Such changes in the lidar ratio are expected to have a corresponding effect on the marine AOD from CALIOP. The outcomes of this study are relevant for future improvements of the SODA and CALIOP operational product and could lead to more accurate retrievals of marine AOD.

# 1 Introduction

Marine aerosols are produced through primary emission of sea spray particles, and oxidation of phytoplankton-produced dimethylsulfide and biogenic volatile organic carbon. Radiative forcing by marine aerosol comprises a significant portion of the global energy budget. Studies have shown that marine aerosol optical depth (AOD) is approximately 0.15 and likewise, the contribution of marine aerosol to cloud condensation nuclei is about  $60 \text{ cm}^{-3}$  (Kaufman et al., 2002; Lewis and Schwartz, 2004). Thus, marine aerosol is an important natural contributor to global aerosol burden affecting both direct (i.e., extinction of solar radiation via scattering and absorption) and indirect (i.e., cloud lifetime and frequency) radiative forcing of climate. As marine aerosols contribute considerably to the preindustrial, natural background and provide the base line on top of which anthropogenic forcing should be quantified, it is very important to properly characterise marine aerosol burden and its spatiotemporal distribution. The incomplete characterisation of background aerosols, of which marine particles are part of, was shown to contribute large uncertainty in anthropogenic aerosol forcing calculations and climate simulations (Ghan et al., 2001; Hoose et al., 2009; Wang and Penner, 2009; Meskhidze et al., 2011; Westervelt et al., 2012; Carslaw et al., 2013).

Aerosols over the remote oceans come from natural continental (e.g., mineral dust and biomass burning) and human-induced pollution (Andreae, 2007) in addition to marine sources. Therefore, knowing horizontal and vertical distribution, as well as speciation of aerosols becomes extremely important for the correct quantification of marine aerosol radiative properties. The last decade has produced a large body of information regarding the sources and composition of marine aerosol, resulting in a reassessment of the complex role that marine aerosols play in climate and various geophysical phenomena. Passive satellite instruments like the Sea-Viewing Wide Field-of-view Sensor (SeaWiFS), the MODerate resolution Imaging Spectroradiometer (MODIS), and the Multi-angle Imaging Spectroradiometer (MISR), as well as the ground-based AEROSOL RObotic NETwork (AERONET) have contributed immensely to quantitative characteristics of marine aerosol in terms of AOD (the column integrated aerosol extinction), size distribution information and spectral optical properties. Although passive instruments have been useful for developing a basic picture of marine aerosol distribution, they supply limited information on aerosol speciation and very little data related to aerosol distribution in the vertical column. The introduction of the Cloud-Aerosol Lidar with Orthogonal Polarization (CALIOP) onboard the Cloud-Aerosol Lidar and Infrared Pathfinder Satellite Observations (CALIPSO) platform has

1 eliminated some of the assumptions made by the passive instruments and has provided a  
2 more complete picture of the global aerosol distribution wanted by climate scientists.  
3 However, CALIOP is an elastic backscatter lidar with no molecular filtering capability and  
4 therefore requires the assumption of an extinction-to-backscatter ratio, also known as the  
5 lidar ratio, to infer extinction from attenuated backscatter measurements. Depending on the  
6 microphysical properties of the aerosol, the lidar ratio can have a wide range of values and  
7 therefore a straightforward a-priori solution within some reasonable uncertainty range is  
8 generally unobtainable without various assumptions or constraints. Theoretical calculations  
9 for the lidar ratio can be performed, if the physicochemical properties and the size  
10 distribution of the particles at the different heights in the vertical column are known;  
11 however, the fulfillment of these requirements would make the lidar measurements  
12 unnecessary (Ackermann, 1998). The typical solution to this problem is to assign a vertically  
13 independent lidar ratio to aerosol retrievals that fit a specific aerosol model as outlined in  
14 Omar et al. (2009).

15 “To date, experimental techniques for directly measuring the lidar ratio include the  
16 use of High Spectral Resolution Lidar (HSRL, Eloranta, 2005; Hair et al., 2008) and Raman  
17 Lidar (RL, Ansmann et al., 1990). These instruments are capable of measuring aerosol  
18 backscatter and extinction parameters independently and therefore do not require the lidar  
19 ratio to be prescribed (e.g., Shipley et al., 1983; Grund and Eloranta, 1991; Piironen and  
20 Eloranta, 1994; Müller et al., 2007; Amiridis et al., 2009; Tesche et al., 2009a,b; Burton et al.,  
21 2012). On the other hand, Catrall et al. (2005) use AERONET size distributions inverted  
22 from sun photometer data (Holben et al., 1998) to calculate the lidar ratio and then compare  
23 their indirect to literature reported direct measurements. They determined that their indirect  
24 method ( $28 \pm 5$ ) compared well to the literature average of direct retrievals ( $29 \pm 5$ ) (see Tables  
25 3 and 4 in Catrall et al., 2005). Direct measurements do not suffer the same limitations as  
26 indirect ones which require assumptions on size distribution and chemical composition or a  
27 molecular extinction profile. The supplementary Table S1 summarises available retrieval  
28 methods and values of some experimentally determined lidar ratios over marine regions.  
29 Currently, most lidars do not yet have Raman or high spectral resolution capability and  
30 CALIPSO is the only lidar that provides aerosol data at the vast spatiotemporal resolution  
31 required for global climate model comparison.”

32 Since the uncertainty in the lidar ratio can significantly affect the accuracy of the  
33 aerosol extinction retrieval (see a detailed discussion below), lidar ratios have been  
34 constrained by numerous approaches. However, marine aerosol size distribution, chemical

1 composition and refractive index can change significantly with ocean surface wind speed  
2 ( $U_{10}$ ), relative humidity (RH), temperature, salinity and chemical/biological composition of  
3 surface sea water (de Leeuw et al., 2011; Lewis and Schwartz, 2004). For this reason, large  
4 disagreement exists in the literature regarding the value of maritime aerosol lidar ratio ( $S_p$ ;  
5 subscript “p” indicates particulate). For example, lidar measurements of (Ansmann et al.,  
6 2001) over the North Atlantic showed  $S_p = 24 \pm 5$  sr whereas measurements using a  
7 nighttime lidar at a horizontal orientation off the northern coast of Queensland, Australia  
8 showed maritime aerosol lidar ratios as high as  $S_p = 39 \pm 5$  (Young et al., 1993). Using the  
9 data from AERONET oceanic sites, Cattrall et al. (2005) derived a lidar ratio of  $28 \pm 5$  sr, a  
10 value that compared well with a literature averaged value of  $S_p = 29 \pm 5$  sr (for  $490 \leq$   
11  $\lambda \leq 550$  nm) for maritime aerosols. Passive techniques have also been used to derive the  
12 lidar ratio using an alternative definition of  $S_p$  as a function of single scattering albedo and  
13 the scattering phase function near  $180^\circ$  (Bréon, 2013). Using the multi-directional  
14 measurements of solar radiation from the polarization sensitive passive radiometer POLDER,  
15 typical values for clean marine aerosol  $S_p$  were derived to be 25 sr at 532 nm (Bréon, 2013).  
16 The lidar ratio of  $20 \pm 6$  sr (at 532 nm) was selected for the CALIOP retrieval algorithm  
17 based on parameters measured during the Shoreline Environmental Aerosol Study (SEAS)  
18 experiment (Masonis et al., 2003; Omar et al., 2009). The SEAS measurements conducted on  
19 the beach (downwind of an offshore reef) report a particulate lidar ratio  $S_p = 25.4 \pm 3.5$  sr  
20 at 532 nm based on the optical size measurements of marine aerosol, and an average modeled  
21 value of  $S_p = 20.3$  sr (Masonis et al., 2003). However, it was also shown that depending on  
22 a particle size and wind speed regime  $S_p$  values can range from 10 to 90 sr (Masonis et al.,  
23 2003; Sayer et al., 2012). Therefore, as size distribution (and chemical composition) of  
24 marine aerosol may vary over the oceans, a constant lidar ratio used in CALIOP algorithms  
25 may lead to erroneous retrievals of AOD.

26 In this study, we present a new method for deriving lidar ratios for individual  
27 CALIOP retrievals of single aerosol layer columns over the ocean. We have used the  
28 Synergized Optical Depth of Aerosols (SODA) product (described in section 2.2) to estimate  
29  $S_p$  for a strictly defined subset of CALIPSO data. The  $S_p$  values are calculated as a  
30 correction to achieve the best agreement between SODA and CALIPSO marine aerosol AOD  
31 values. Using CALIPSO level 2 aerosol layer data for years 2007 to 2010, we have created a  
32 3-year averaged climatology of clean marine aerosol lidar ratio over the globe. Analyses were  
33 also carried out to assess dependence of  $S_p$  values on wind speed and estimate possible error

1 sources in our calculations.

## 2 **2 Instrumentation and Methods**

### 3 **2.1 CALIPSO satellite**

4 The CALIPSO mission (Winker et al., 2009), launched on April 28, 2006, has been able to  
5 provide the scientific community with vertically resolved measurements of both aerosol and  
6 cloud optical properties like depolarization ratio (a measure of particle sphericity), AOD, and  
7 ice/water phase since June 2006. The CALIPSO payload includes a high-powered digital  
8 camera, an infrared radiometer, and a two-wavelength (532 and 1064 nm), near nadir,  
9 polarization sensitive, elastic backscatter lidar, CALIOP.

10 The level 1 data algorithms are responsible for the geolocation and range  
11 determination of the satellite and produce profiles of attenuated backscatter coefficients. Data  
12 in this work were obtained from the 5 km, level 2 operational products version 3.01. Level 2  
13 products have undergone various processing algorithms from the Selective Iterated BoundarY  
14 Locator (SIBYL), the Scene Classification Algorithm (SCA), and the Hybrid Extinction  
15 Retrieval Algorithm (HERA) (Vaughan et al., 2004; 2009). First, SIBYL identifies layers,  
16 then the SCA identifies the type of feature (i.e., aerosol or cloud) and the subtype (i.e.,  
17 aerosol type, ice/water phase), and finally, the HERA generates extinction profiles for the  
18 feature. The theoretical basis of the algorithm can be found online at  
19 [www-calipso.larc.nasa.gov/resources/project\\_documentation.php](http://www-calipso.larc.nasa.gov/resources/project_documentation.php).

20 The CALIPSO 5 km aerosol layer data includes many operational products of which  
21 only a few are used in this study. Among them are, the integrated attenuated backscatter  
22 and its uncertainty at 532 nm, the layer features such as number found in the column and their  
23 top and bottom altitudes and the feature classification flags.

### 24 **2.2 Synergized Optical Depth of Aerosols (SODA)**

25 CloudSat was launched in 2006 with CALIPSO and was positioned in sun-synchronous orbit  
26 as part of the A-Train satellite constellation. CloudSat and CALIPSO have paved the way for  
27 new multi-sensor data products like SODA to be developed. The main instrument on  
28 CloudSat is the Cloud Profiling Radar (CPR), a nearly nadir looking ( $0.16^\circ$ ) 94-GHz ( $\approx 3$   
29 mm; W-band) radar. The CPR, like CALIOP, can retrieve information on hydrometeor  
30 microphysical properties at different heights in a vertical column. The CPR signal is mostly

1 attenuated by water vapor; however, for cloud free regions over the ocean, the CPR data can  
 2 be used to retrieve AOD. A method developed by Josset et al. (2008) and later expanded by  
 3 Josset et al. (2010a) uses a combination of CALIOP and CPR measurements of the ocean  
 4 surface reflectance to derive AOD. The design of SODA utilises the ratio of the radar-to-lidar  
 5 ocean surface scattering cross section to infer column optical depth for non-cloudy  
 6 atmospheric columns. Since the radar signal attenuates mostly due to water vapor and the  
 7 lidar signal weakens mostly due to aerosols, after the radar signal is corrected for attenuation  
 8 by water vapor and oxygen, the change in the radar-to-lidar signal ratio is directly related to  
 9 aerosol abundance (Josset et al., 2008; 2010a). Therefore, by using observations from two  
 10 different sensors, SODA can eliminate uncertainties induced by the CALIOP aerosol  
 11 extinction algorithm over oceans. SODA AODs have been shown to be in very good  
 12 agreement with MODIS AOD retrievals (Josset et al., 2008). A more detailed description of  
 13 the SODA technique and its application is given in Josset et al. (2008; 2010a; 2010b; 2011;  
 14 and 2012). The SODA products that are used in this study include the quality assurance  
 15 measure "qa\_flag\_aerosol" and the 532 nm AOD.

## 16 2.3 Lidar ratio definition

17 One of the biggest advantages of the SODA product is that it removes the dependence of the  
 18 prescribed lidar ratio while still utilizing the active sensors to retrieve an AOD, thereby  
 19 providing a means for independent evaluation of the lidar ratio. In the current study we use  
 20 Eq. 4 from Josset et al. (2011) to estimate lidar ratio from CloudSat/CALIOP measurements  
 21 of AOD values. Following Fernald et al. (1972), the particulate two-way transmittance at  
 22 height  $Z$  can be written as:

$$T^2(Z) = e^{-2S_p \int_0^Z \beta_p(z) dz} \quad (1)$$

23 where the lidar ratio at height  $Z$  can be defined as the ratio of the particulate extinction to  
 24 backscatter  $\left(S_p = \frac{\sigma_p(Z)}{\beta_p(Z)}\right)$ . Differentiating Eq. 1 with respect to vertical coordinate ( $z$ ) gives  
 25 the particulate backscatter at height  $Z$ :

$$\beta_p(Z) = -\frac{1}{2S_p T^2(Z)} \frac{dT^2(Z)}{dZ} \quad (2)$$

26 Since atmospheric constituents (molecules and different particle types) can interact with the  
 27 lidar beam at different heights, the lidar ratio using remotely sensed data cannot be uniquely  
 28 defined for a given atmospheric column. However, the lidar ratio is a particle intensive  
 29 property (i.e., dependent on particle type and not on the amount). So, if we assume that there

1 is only a single type of aerosol and it is homogeneously distributed throughout the  
 2 atmospheric column and that molecular scattering is sufficiently removed by the CALIOP  
 3 level 2 algorithms, then the column lidar ratio ( $\overline{S}_p$ ) can be expressed as the ratio of the  
 4 particulate column integrated extinction ( $\overline{\tau}_p = \text{AOD}$ ) to the attenuated backscatter ( $\overline{\Gamma}_p$ ). Based  
 5 on these assumptions, integration of Eq. 2 with respect to vertical coordinate gives the  
 6 particulate lidar ratio as:

$$\overline{S}_p = \frac{\int_{T_p^2(0)}^{T_p^2(z)} dT^2(z)}{\int_0^z \beta_p(z) T_p^2(z) dz} \quad (3)$$

7 If we first substitute in Eq. 3 the definition for two-way transmittance as  $T_p^2 = e^{-2\overline{\tau}_p}$ , then  
 8 substitute the total particulate attenuated backscatter signal retrieved by the lidar as  
 9  $\overline{\Gamma}_p = \int_0^z \beta_p(z) T_p^2(z) dz$  and finally consider that  $T_p^2(0) = 1$ , the equation for a columnar  
 10 particulate lidar ratio is:

$$\overline{S}_p = \frac{1 - e^{-2\overline{\tau}_p}}{2\overline{\Gamma}_p} \quad (4)$$

11 Equation 4 allows us to calculate marine aerosol lidar ratio from two independent sources: the  
 12 AOD (i.e.,  $\overline{\tau}_p$ ) from SODA and the integrated attenuated backscatter ( $\overline{\Gamma}_p$ ) from CALIOP. It  
 13 should be noted that CALIOP estimation of  $\overline{\Gamma}_p$  is difficult for layers that are not bounded by  
 14 clear air (Vaughan et al., 2004) and therefore require carefully designed data screening  
 15 algorithms. In section 4 we carry out an error analysis to verify that uncertainties in  $\overline{\Gamma}_p$  have  
 16 a minimal effect on the retrieved lidar ratio.

## 17 2.4 Data selection method

18 As different aerosol sub-types have different lidar ratios, application of Eq. 4 to episodes  
 19 when aerosols other than marine aerosols are present in the atmospheric column may lead to  
 20 erroneous results for the calculated  $\overline{S}_p$ . We developed a strict scene selection algorithm to  
 21 minimise the contamination of AOD and therefore  $\overline{S}_p$  by aerosol types other than marine  
 22 (e.g., anthropogenic pollution, biomass burning, and dust). The algorithm first uses the  
 23 feature classification flags in the CALIOP aerosol layer product. We start with clean marine  
 24 aerosol that is identified based on surface type (as determined by the location of the satellite)  
 25 and then retain only the data with total integrated attenuated backscatter  $\gamma' < 0.01 \text{ km}^{-1}\text{sr}^{-1}$   
 26 and volume depolarization ratio  $\delta' < 0.05$  (Omar et al., 2009). As multiple types of aerosols

1 can be found within retrieved vertical profiles (e.g., dust above marine aerosols), aerosol  
 2 feature types that have been identified as marine in a given atmospheric column are not  
 3 enough to carry out the analysis. Therefore, when determining the lidar ratio of marine  
 4 aerosol using Eq. 4, the algorithm only retains the data in which clean marine is the only type  
 5 of aerosol present in the entire cloud-free atmospheric column. To further reduce the  
 6 uncertainty, we constrain the analysis to single layer profiles below 2 km and remove profiles  
 7 in which marine aerosol layers are vertically stacked within an atmospheric column.  
 8 Therefore, the vertically integrated particulate attenuated backscatter  $\overline{\Gamma_p}$  is replaced by  $\Gamma_p$ .  
 9 Similarly, the column lidar ratio  $\overline{S_p}$  is reduced to  $S_p$  in the remainder of the text. Note also  
 10 that all quantities discussed are particulate quantities and therefore, molecular scattering is  
 11 removed using gridded molecular and ozone number density profile data from the Goddard  
 12 Earth Observing System Model, version 5 (GEOS-5) analysis product available from the  
 13 NASA Global Modeling and Assimilation Office (GMAO) (Winker et al., 2009).  
 14 Operationally, particulate scattering is determined to be where the ratio of the CALIOP 532  
 15 nm scattering profile normalised by the GEOS-5 molecular scattering profile is greater than  
 16 one ( $\frac{\beta'_{532}}{\beta_m} > 1$ ). Errors associated with  $\overline{\Gamma_p}$  are discussed in Sec. 4.

17 All data is for nighttime and is binned into  $2^\circ \times 5^\circ$  latitude and longitude, respectively,  
 18 grid cells. Collocated wind speed is taken from the Advanced Microwave Scanning  
 19 Radiometer - Earth (AMSR-E) observing system. To identify distinct features associated with  
 20 the variability in marine aerosol lidar ratio over different parts of the oceans, the selected data  
 21 is examined in relation with other variables such as season, spatial location and wind speed.

22 Some additional measures were taken to target layers with a high signal-to-noise ratio  
 23 and grid cells with a significant number of observations. These measures included (i)  
 24 ensuring the relative error in  $\Gamma_p$  due to random noise in molecular backscatter was  $< 50\%$ ,  
 25 (ii) the collocated SODA 5 km layer was composed of at least 70% shot-to-shot data and (iii)  
 26 the total number of retrievals per  $2^\circ \times 5^\circ$  grid cell ranked above the first quartile of the grid  
 27 cell frequency distribution. Such strict quality controls considerably increase the reliability of  
 28 the analysis despite reducing the total number of data points. It should be noted that a large  
 29 number (over 260,000) of data points remained for robust statistics after all the quality  
 30 control and quality assurance tests. A caveat, despite such rigorous quality control criteria,  
 31 remains when interpreting data near coastlines as the CALIOP scene classification algorithm  
 32 may mistakenly identify mixtures of continental pollution and marine as clean marine aerosol  
 33 (Burton et al., 2013; Oo and Holz, 2011; Schuster et al., 2012) causing an overestimation in



1 the lidar ratio inferred from Eq. 4. Further discussion of error analysis is given in Sec. 4.

2

### 3 **3 Results**

#### 4 **3.1 Global distribution of retrieved AOD and lidar ratio**

5 Active detectors like CALIOP require knowledge of the lidar ratio for retrieval of  
6 aerosol optical properties. Incorrect estimates of the  $S_p$  values for a given aerosol type can  
7 lead to significant errors in the retrievals of particulate extinction and AOD. Past studies  
8 using collocated CALIOP and MODIS retrievals have shown that, over the marine regions,  
9 CALIOP underestimates the AOD values relative to MODIS (Oo and Holz, 2011). As  
10 MODIS data over the ocean has been extensively evaluated with numerous field campaigns  
11 (e.g., Levy et al., 2005), it was suggested that the primary source of discrepancy between the  
12 two sensors was the low value of the marine aerosol lidar ratio used by CALIOP (Oo and  
13 Holz, 2011). Figure 1 shows seasonally averaged maps of CALIPSO and SODA marine  
14 aerosol median optical depth at 532 nm and the differences between SODA and CALIOP  
15 retrieved AODs. White regions on Fig. 1 represent grid cells that were rejected by the data  
16 selection algorithm and have been removed from the subsequent data analysis. Inspection of  
17 Fig. 1 reveals considerable spatial and temporal variations in marine aerosol AOD. Although  
18 the largest values of AOD seem to occur over regions with higher surface wind speed (i.e.,  
19 the northern and southern oceans), elevated AOD values can also be seen over the regions  
20 downwind from dust and/or pollution sources such as the mid-latitude North Atlantic Ocean  
21 and the Bay of Bengal and over the major oceanic gyres. The region around the Indian  
22 subcontinent and over the Bay of Bengal is believed to be just a retrieval artifact. Large  
23 disagreements between SODA and CALIOP reported AODs for these regions suggest that  
24 some dust/pollution aerosols might have been misclassified by CALIOP as marine aerosol.  
25 Higher  $S_p$  values for dust and pollution compared to marine aerosol would produce a higher  
26 AOD retrieval in SODA compared to CALIOP. Elevated AOD values over the oceanic  
27 regions with lower surface wind speed, on the other hand, could point to changes in marine  
28 aerosol size distribution to smaller sizes. Sub-micron sea salt aerosols (with particle diameter,  
29  $D_p < 1 \mu\text{m}$ ) are believed to have larger lidar ratios than super-micron ones (e.g., Masonis et  
30 al., 2003; Oo and Holz, 2011). In general, Fig. 1 shows positive differences between SODA  
31 and CALIOP retrieved seasonal median AOD values. Recalling that CALIOP retrieved  
32 extinction is the product of the prescribed lidar ratio and the measured column integrated

1 particulate backscatter, positive differences between SODA and CALIOP median AODs at  
2 532 nm over most of the oceans suggest underestimation of the marine aerosol lidar ratio  
3 prescribed in the CALIOP clean marine aerosol model. Figure 2 shows that over most of the  
4 ocean surfaces, the calculated lidar ratio is higher than the default ( $S_p = 20$  sr) used in the  
5 CALIOP clean marine aerosol model. Global means and standard deviations for AOD and  
6 lidar ratio are given in Table 1. CALIOP retrievals in this study cannot be directly compared  
7 to MODIS since we only use nighttime data. Nevertheless, SODA retrievals of AOD have  
8 been shown to agree well with MODIS (Josset et al., 2008), HSRL (Fig. 7a; Josset et al.,  
9 2011) and Maritime Aerosol Network (Smirnov et al., 2011; Fig. 8) observations suggesting  
10 that the corrected lidar ratios will bring CALIOP retrievals close to MODIS data. Figure 2  
11 also reveals that the value of the lidar ratio calculated using Eq. 4 changes considerably over  
12 different parts of the remote oceans, pointing to the variability in marine aerosol optical  
13 properties. It has long been known that meteorological and/or environmental factors and  
14 ocean chemical/biological composition influence marine aerosol production, entrainment,  
15 transport, and removal processes (Lewis and Schwartz, 2004) that can ultimately affect  
16 marine aerosol  $S_p$ . Moreover, due to atmospheric transport of marine aerosol, satellite  
17 retrieved AOD values may also be related to the upwind processes. Despite the complexity of  
18 the mechanisms controlling marine aerosol mass concentration over the oceans, surface wind  
19 speed has always been considered as the major parameter governing the production, chemical  
20 composition, and life cycle of marine aerosol (Lewis and Schwartz, 2004). Therefore, in the  
21 next section we will investigate the effect of wind speed on calculated temporal variability of  
22 marine aerosol lidar ratio.

### 23 3.2 Wind speed dependence

24 Numerous investigators have examined the effect of sea surface wind speed and sea state on  
25 marine aerosol optical properties (e.g., Smirnov et al., 2003; Sayer et al., 2012). There are  
26 two mechanisms for primary marine aerosol production: bursting of bubbles at the water  
27 surface, and mechanical tearing of water drops (spume) from wave crests (for surface wind  
28 speeds  $U_{10} > 9$  ms<sup>-1</sup>, Anguelova et al., 1999). Ocean bubbles are generated by the  
29 entrainment of air due to wave action. As bubbles rise due to their buoyancy, they burst at the  
30 surface producing marine aerosol (Blanchard and Woodcock, 1957). In this study we have  
31 selected seven different wind speed regimes (see Table 2). The lowest wind speed regime,  
32  $0 < U_{10} \leq 4$  ms<sup>-1</sup>, was chosen to represent aerosols not generated via wind driven processes

1 over the ocean. In general, ocean waves break at wind speed values above  $\sim 4 \text{ ms}^{-1}$  (initiating  
2 the white cap formation and bursting of the entrained bubbles) (Lewis and Schwartz, 2004).  
3 Therefore, it has been suggested that below this threshold value, there should be a weak  
4 relationship between marine aerosol optical properties and the surface wind speed  
5 (Kiliyanpilakkil and Meskhidze, 2011; Lehahn et al., 2010). Moreover, for such a low wind  
6 speed regime, most of the aerosols classified as clean marine by CALIOP are either produced  
7 outside the swath and then blown into the satellite field of view, or like in cases near  
8 coastlines, mistakenly identified as marine aerosol. The highest wind speed regime, with  $U_{10}$   
9  $> 15 \text{ ms}^{-1}$ , typically contributes a small fraction of CALIOP retrievals (Kiliyanpilakkil and  
10 Meskhidze, 2011) and is largely concentrated over the southern ocean and in the northern  
11 Atlantic where the highest wind speeds are observed (Bentamy et al., 2003). Figure 3 shows a  
12 spatial map of the number of retrievals for each grid cell separated by wind speed regime.  
13 According to Fig. 3 the southern ocean retrievals are dominant at the highest wind speeds and  
14 are overall consistent with the so-called “roaring 40s” latitude band. Figure 3, as well as  
15 Table 2, shows that the fewest number of retrievals are found for the lowest and highest wind  
16 regimes.

17 The data shown in Fig. 3 are next used to generate scatter density plots for SODA and  
18 CALIOP retrieved AOD values for the wind speed regimes reported in Table 2 (see Fig. 4).  
19 As expected, Fig. 4 shows that increases in wind speed are typically associated with higher  
20 values of marine aerosol optical depth (note the center of the scatter distribution shifts  
21 slightly to higher AODs for larger wind speed values). However, as the majority of the  
22 SODA AODs exist above the 1:1 line, this figure also indicates the underestimation of  
23 CALIOP retrieved marine aerosol optical depth values. When averaged over the entire globe,  
24 CALIOP retrieved clean marine AOD is roughly 32% lower compared to SODA (with an  
25 RMS error of 0.06; supplementary Fig. S2). According to Fig. 4 the largest discrepancies  
26 between SODA and CALIOP retrievals are observed at lower wind speed values. One simple  
27 explanation for this is a greater chance for CALIOP misclassification over the oceanic  
28 regions where long-ranged continental aerosols can contribute a larger fraction of the MBL  
29 particles (e.g., Blot et al., 2013). Terrestrial particles (e.g., mineral dust, anthropogenic  
30 pollution) are typically characterised by the larger lidar ratio values, leading to an  
31 underestimation of the CALIOP retrieved AODs. However, measurements also show that  
32 changes in surface wind speed values can cause a considerable shift in the marine aerosol size  
33 distribution. For optically active marine aerosols, the residence time decreases considerably  
34 with increasing size. Thus the aerosol population is increasingly controlled by the smaller end

1 of the particle size spectrum as wind speeds decrease over the ocean (Hoffman and Duce,  
2 1974). Conversely, as wind speed increases, fine mode aerosol volume size distribution  
3 changes slightly (with mixed trends), while the coarse mode volume size distribution exhibits  
4 a large and positive response to the increase in wind speed (Lewis and Schwartz, 2004;  
5 Smirnov et al., 2003). Such variability in marine aerosol volume size distribution is expected  
6 to have an effect on the aerosol lidar ratio. As sub-micron marine aerosols are characterised  
7 with much larger lidar ratios than super-micron ones (e.g., Masonis et al., 2003; Oo and Holz,  
8 2011), shifting marine aerosol size distribution spectra to smaller particles will cause an  
9 increase in total aerosol lidar ratio. Therefore, for clean MAs, AODs and lidar ratios are  
10 expected to have opposite dependences on wind speed: high wind speed regions are  
11 characteristic of high AODs and low lidar ratios while lower wind speeds favor higher lidar  
12 ratios and lower AODs (Smirnov et al. 2003; Sayer et al., 2012).

13 Figure 5 shows that on average, the calculated aerosol lidar ratio is weakly related to  
14 the surface wind speed. According to this figure, aerosols retrieved in the wind speed regime  
15  $0 < U_{10} \leq 4 \text{ ms}^{-1}$  depict the largest variability in the lidar ratio as indicated by the spread of  
16 the distribution. As discussed above, aerosols in this regime likely include both marine  
17 aerosols particles produced upwind and advected into the satellite field of view (with  $S_p \sim$   
18 20 to 30 sr), as well as dust/pollution particles (with  $S_p \sim 40$  to 70 sr, Omar et al., 2009) that  
19 may have been misclassified by CALIOP as marine aerosol. As shown in Table 2, marine  
20 aerosol lidar ratio distribution in this regime is characterised by the largest standard deviation  
21 ( $\sigma = 17.4 \text{ sr}$ ) indicating that for the lowest wind speed values, a wide range of marine  
22 aerosol sizes can be present over the ocean. Since for the wind speed values less than  $4 \text{ m s}^{-1}$ ,  
23 the primary marine aerosol production is minimal, such large spread could also indicate that  
24 under low wind conditions there is greater probability for natural continental and  
25 human-induced pollution aerosols be miss-classified by CALIOP as clean marine.

26 For the higher wind speed values ( $4 < U_{10} \leq 15 \text{ ms}^{-1}$ ) lidar ratio generally decreases  
27 with the increase in the wind speed and approaches the lidar ratios prescribed by CALIOP  
28 retrieval algorithms (i.e., 20 sr) at the highest wind speed regime. According to Table 2 and  
29 Fig. 3, the most common wind values in CALIOP marine aerosol retrievals over the ocean  
30 are in the  $8 < U_{10} \leq 10 \text{ ms}^{-1}$  regime (26% of all available data) followed by the  $6 < U_{10} \leq$   
31  $8 \text{ ms}^{-1}$  regime (23% of all available data). For the higher wind speed regimes ( $U_{10} \gtrsim$   
32  $6 \text{ ms}^{-1}$ ), surface winds play a decisive role in the determination of the lidar ratio (indicated  
33 by the narrow standard deviation, see Table 2). This is an important result as the distributions

1 shown in Fig. 5 may help in providing additional criteria for clean marine lidar ratio  
2 selection, yielding improved retrievals of marine aerosol AOD from CALIOP.

3 Analysis of data indicates that a mean lidar ratio of 26 sr is the most probable value  
4 that occurs for the majority of CALIOP retrievals over the oceans. This value compares well  
5 with those reported in the literature. Müller et al. (2007) found a marine aerosol lidar ratio of  
6  $23 \pm 3$  and  $23 \pm 5$  sr using RL and Burton et al. (2012; 2013) reported a range from 15-27 sr  
7 using HSRL. Bréon (2013) used a different space-based retrieval and saw  $S_p$  for marine  
8 aerosol is typically on the order of 25 sr. Table S1 reports some additional values of marine  
9 aerosol  $S_p$  measured by other techniques. This new lidar ratio reduces discrepancy between  
10 CALIOP-prescribed and SODA-derived lidar ratios from about 30% to 4%.

11 Previous studies reported a small decrease in marine aerosol lidar ratio with the  
12 increase in wind speed (Sayer et al., 2012). In general, wind speed alone is expected to be a  
13 poor predictor of marine aerosol lidar ratio, as aerosol volume size distribution and optical  
14 properties are likely to be influenced by a number of other parameters including relative  
15 humidity and marine boundary layer depth. Furthermore, errors increase exponentially  
16 approaching the lowest optical depths and could be the reason for the large spread in the lidar  
17 ratio seen in Fig. 5. Untangling systematic error from real physical effects is difficult in the  
18 low (0-4 m/s) wind speed regime and highlights the need for more accurate measurements for  
19 calm wind/low AOD conditions. Despite these complications, a shift to lower lidar ratios  
20 with increasing wind speed can be seen from Fig. 5 and warrants further investigation.

## 21 **4 Uncertainties, errors and sensitivity**

22 The method used to derive the lidar ratio in this study depends on two parameters: the  
23 CALIOP integrated attenuated particulate backscatter ( $\Gamma_p$ ) and the SODA aerosol optical  
24 depth ( $\tau_p$ ). Uncertainties in both  $\Gamma_p$  and  $\tau_p$  retrievals are expected to propagate through  
25 the calculations of the particulate lidar ratio. Josset et al. (2008; 2010a) investigate the  
26 domain of validity for  $\tau_p$  through an extensive calibration procedure. They find that for  
27 retrievals at wind speeds between 3 and 10  $\text{ms}^{-1}$  the SODA product is in very good agreement  
28 ( $R > 0.89$ ) with MODIS AOD with calibration errors less than 15%. Calibration errors in  
29  $\tau_p$  are expected to be even lower for nighttime retrievals used in this study (Josset et al.  
30 2008). On the other hand, average uncertainty for CALIOP  $\Gamma_p$  retrievals has not yet been  
31 examined and is necessary for the assessment of this retrieval method. We make an estimate

1 on this uncertainty in the following section.

2 Since ocean is the source of marine aerosol, clean marine aerosol layers typically  
 3 extend to the ocean surface. This makes it more difficult to determine molecular and  
 4 particulate backscatter components of the signal separately using satellite measurements  
 5 alone. To assess the uncertainty in lidar ratio introduced for the surface connected layers (i.e.,  
 6 layers whose bottom bound is defined as the ocean surface), here we estimate the error in  
 7 CALIOP retrieved  $\Gamma_p$  values. The total attenuated backscatter signal measured by the lidar  
 8 consists of molecular and particulate components:

$$\beta_{att} = (\beta_p + \beta_m) e^{-2\tau_p} \cdot e^{-2\tau_m} \quad (5)$$

9 with subscripts  $m$  and  $p$  representing molecular and particulate quantities, respectively. From  
 10 the definition of  $\Gamma_p$  it follows that:

$$\Gamma_p = \int_0^Z \beta_p(z) e^{-2\tau_p} dz \quad (6)$$

11 where the integration is from the surface to the top of the layer.  $\beta_p$  is the particulate  
 12 backscatter and  $e^{-2\tau_p}$  accounts for the attenuation of the lidar signal by the particles.  
 13 Substituting Eq. 5 into Eq. 6 gives:

$$\Gamma_p = \int_0^Z (\beta_{att} e^{2\tau_m} - \beta_m(z) e^{-2\tau_p}) dz \quad (7)$$

14 The molecular component of the signal in Eq. 7 can be derived from the GMAO modeled  
 15 temperature and pressure profiles (Bloom et al., 2005). However, to solve this equation and  
 16 determine the particulate attenuated backscatter value, particulate column integrated  
 17 extinction is required. To get  $\tau_p$  the CALIOP algorithm is using a prescribed value of the  
 18 lidar ratio, making Eq. 4 circularly dependent on the lidar ratio. The error in CALIOP  
 19 retrieved  $\Gamma_p$  associated with the prescribed lidar ratio can be estimated by substituting the  
 20  $\tau_p$  value from SODA. If the error is large, that would imply that the uncertainty in CALIOP  
 21 prescribed lidar ratio would introduce sizable corrections to  $\Gamma_p$ , making Eq. 4 unsuitable for  
 22 the estimation of marine aerosol lidar ratio.

23 The relative error in  $\Gamma_p$  can be defined as:

$$Error = \frac{\Gamma_{p,S} - \Gamma_{p,C}}{\Gamma_{p,C}} = \frac{(e^{-2\tau_{p,C}} - e^{-2\tau_{p,S}}) \cdot \int_0^Z \beta_m(z) dz}{\Gamma_{p,C}} \quad (8)$$

24 where  $\Gamma_{p,S}$  and  $\Gamma_{p,C}$  are columnar integrated attenuated backscatter values for SODA and  
 25 CALIOP, respectively. From the theoretical basis documents for CALIOP level 1 algorithms,

1 the molecular backscatter is estimated as  $\beta_m = \frac{C_s T(z)}{S_m P(z)}$  where height dependent  $T(z)$  and  
 2  $P(z)$  profiles from the surface (1000 hPa) to top-of-atmosphere (0.1 hPa) pressure levels were  
 3 obtained from the GMAO Modern-Era Retrospective analysis for Research and Applications  
 4 dataset. The molecular lidar ratio,  $S_m$  is defined as  $8\pi/3$  and  $C_s$  is a constant equal to  
 5  $3.742 \times 10^{-6}$  K/hPa/m (Hostetler et al., 2005). When considering all of the parameters, our  
 6 analysis shows that the average error in  $\Gamma_p$  is approximately 1.5%. Compared to the  
 7 systematic uncertainty in the SODA product ( $< 15\%$ ), the uncertainty in  $\Gamma_p$  is much lower  
 8 indicating that, on average, errors in  $\Gamma_p$  do not dominate  $S_p$  retrievals. Since an average  
 9 discrepancy between CALIOP-prescribed and SODA-derived lidar ratios ( $\sim 30\%$ ) is more  
 10 than an order of magnitude higher than uncertainty in  $\Gamma_p$ , we conclude that the uncertainty in  
 11 the CALIOP column integrated backscatter has a minor effect on the Eq. 4 calculated lidar  
 12 ratio.

13 Furthermore, because in our study we use feature-integrated products for a single  
 14 aerosol layer, it is also important to evaluate the relationship between  $\Gamma_p$  and aerosol layer  
 15 thickness ( $\Delta Z$ ). Figure 6 shows the normalised column attenuated particulate backscatter  $\Gamma_p$   
 16 as a function of layer depth. For uniformly distributed aerosols throughout the column,  $\Gamma_p$  is  
 17 likely to be proportional to  $\Delta Z$ . The spread of  $\Gamma_p/\Delta Z$  ratio is indicative of different amounts  
 18 of marine aerosol present in the column. Two limits of very high and very low  $\Delta Z$  values are  
 19 of particular interest. For example, strong reduction of the  $\Gamma_p/\Delta Z$  ratio at the higher  $\Delta Z$   
 20 values would indicate that the lidar signal is strongly attenuated throughout the layer reaching  
 21 a sensitivity limit. On the other hand, considerable increase of the ratio for the thin layers  
 22 may indicate contamination of the backscattered signal by strong surface reflectance.  
 23 According to Fig. 6 for the vast majority of the data, signal attenuation and surface  
 24 reflectance do not seem to be major issues for the surface connected layers, suggesting that  
 25 the quality control algorithm described in Sec. 2.4 was sufficient to remove the majority of  
 26 erroneous measures of  $\Gamma_p$ .

27 To further assess the reliability of SODA marine aerosol product we also compared  
 28 collocated HSRL (Fig. 7) and Maritime Aerosol Network (MAN) (Fig. 8) AODs to SODA.  
 29 Figure 7a shows results from three CALIPSO (and therefore SODA) underflights validated  
 30 against HSRL. According to Fig. 7a for AODs  $< 0.3$  (comprising the majority of marine  
 31 aerosol retrievals), SODA compares reasonably well to HSRL ( $R^2 = 0.82$ ,  $RMSE = 0.04$ ;  
 32 similar to the MAN comparison with  $RMSE = 0.03$  in Fig. 8.). Additionally, Fig. 7b

1 illustrates that the relative uncertainty in the SODA retrieved  $S_p$  is typically below 50% for  
2 AODs  $> 0.05$ . In our study, the bulk of AODs measured by SODA (98%) exceed this value  
3 under the quality control criteria discussed in Sec. 2.4. Errors were estimated based on Eq. 15  
4 in Josset et al. (2012) and for AODs  $> 0.05$ , we expect lidar ratio retrieval uncertainties below  
5 50%. Maritime aerosol network and SODA collocation for Fig. 8 was determined based on a  
6 scheme in Smirnov et al. (2011) and Kleidman et al. (2010). We required that the SODA  
7 retrieval be within  $\pm 30$  minutes of the MAN retrieval as well as within a circle with radius of  
8 25 km around the MAN measurement. A map of the retrieval locations and the details of the  
9 algorithm used are given in the supplementary information (Fig. S1). There were 51 matching  
10 MAN data points that passed the collocation screening. The MAN data corresponding to the  
11 same SODA retrieval were averaged and used to generate the scatter plot of MAN and SODA  
12 comparison (Fig. 8). The error bars on Fig. 8 indicate the maximum and minimum values of  
13 the MAN AOD reported for the closest SODA retrieval. Figure 8 shows that in general there  
14 is a good agreement between SODA and MAN retrievals with the data points located  
15 reasonably close to the 1:1 line. The correlation is 0.59 and the RMS error is 0.03.

## 16 **5 Conclusions**

17 A new method showing that it is possible to infer lidar ratios of marine aerosol over the ocean  
18 using two independent sources: the AOD from Synergized Optical Depth of Aerosols  
19 (SODA) and the integrated attenuated backscatter from Cloud-Aerosol Lidar with Orthogonal  
20 Polarization (CALIOP) has here been applied. The proposed equation calculates particulate  
21 lidar ratio for individual CALIOP retrievals of single aerosol layer columns as a correction to  
22 achieve the best agreement between SODA and CALIOP retrievals. The new method allows  
23 calculating marine aerosol lidar ratio and assessing its spatiotemporal variability and  
24 dependence on ocean surface wind speed. Analyses were carried out using CALIOP level 2,  
25 5km aerosol layer and collocated SODA nighttime data from December 2007 to November  
26 2010. During the data analysis over 260,000 data points passed various quality-control and  
27 quality-assurance tests to reduce errors associated with the clean marine aerosol retrievals.  
28 The calculated lidar ratios have been analysed over the global ocean covering a wide range of  
29 wind speed and AOD conditions. Data analysis shows that over most of the ocean surfaces,  
30 the calculated lidar ratio is higher than the default lidar ratio of 20 sr used in the CALIOP  
31 clean marine aerosol model. The calculated aerosol lidar ratios are inversely related to the  
32 surface wind speed. Increases in mean surface ocean wind speeds from 0 to  $>15 \text{ ms}^{-1}$  reduces



1 the mean lidar ratio for marine aerosol from ~32 sr to ~22 sr. Such reduction was explained  
2 by the shift in aerosol volume size distribution with the wind speed; however, it was also  
3 emphasised that future studies should explore the role of meteorological and/or  
4 environmental factors and ocean chemical/biological composition for marine aerosol  
5 intensive properties. Our data analysis showed that changes in wind speed also affect the  
6 probability density function for marine aerosol lidar ratio distribution. The largest standard  
7 deviation calculated for the lowest wind speed regime suggested that under low wind  
8 conditions, a wide range of marine aerosol sizes can be present over the ocean and there is  
9 greater probability for natural-continental and human-induced pollution aerosols to be  
10 classified by CALIOP as clean marine. We would like to mention that the role of organic  
11 aerosol at low wind speeds is still unclear. A large body of experimental data suggests that  
12 increases in the organic fraction of marine aerosol can have implications on hygroscopicity  
13 (e.g. Saxena et al., 1995; Fuentes et al., 2011; Ovadenevaite et al., 2013) and could  
14 potentially influence our results. Overall, our data analysis shows that an average value of 26  
15 sr for clean marine aerosol lidar ratio provides the best agreement between the SODA product  
16 and CALIOP retrieved global mean marine aerosol optical depth values. However, our study  
17 also shows large spatiotemporal variability in marine aerosol lidar ratios, suggesting that a  
18 single constant value of the lidar ratio is not suitable for a wide range of marine aerosol and  
19 can lead to large uncertainties at different locations and seasons.

20 We have estimated the error in CALIOP retrieved column integrated attenuated  
21 particulate backscatter. Calculations suggest that the average uncertainty in particulate  
22 backscatter is more than an order of magnitude lower compared to the retrieved value. Data  
23 analysis also showed no clear indication for either approaching a sensitivity limit (due to  
24 strong attenuation of the lidar signal throughout the layer) or the contamination of the  
25 backscattered signal by the surface reflectance. Based on the conducted error analysis we  
26 conclude that the strict quality control criteria developed in this study is adequate to remove  
27 the majority of erroneous retrievals.

28 Finally, even though calculations here were carried out for marine aerosol, the  
29 technique used in this study is broad and can be used to infer lidar ratios of different species  
30 of atmospheric aerosols (i.e., mineral dust, biomass burning, etc.) advecting over the ocean.  
31 Because our data analysis shows that it is possible to derive a correction to the CALIOP  
32 prescribed marine aerosol lidar ratio, future studies should also consider conducting case  
33 studies over different oceanic regions to examine the possible effects of meteorological  
34 parameters and ocean physiochemical/biological composition on marine aerosol lidar ratio.

1 Classification of the spatiotemporal distribution and wind speed dependence of a limited  
2 number of parameters affecting marine aerosol lidar ratios may lead to improved retrievals of  
3 AOD values over the oceans.

4

## 5 **Acknowledgements**

6 This research was supported by the National Aeronautics & Space Administration (NASA)  
7 through grant numbers NNX11AG72G and NNX14AL89G, and by the National Science  
8 Foundation through the grant AGS-1249273. The authors gratefully acknowledge the  
9 CALIPSO, CloudSat, and NASA Langley HSRL Teams for their support and effort in  
10 making the data available. CALIPSO data were obtained from the NASA Langley Research  
11 Center Atmospheric Science Data Center. CloudSat data are produced by Remote Sensing  
12 Systems and sponsored by the NASA Earth Science MEaSUREs DISCOVER Project and the  
13 Advanced Microwave Scanning Radiometer (AMSR-E) Science Team. The SODA product is  
14 developed at the ICARE data and services center (<http://www.icare.univ-lille1.fr>) in Lille  
15 (France) in the frame of the CALIPSO mission and supported by CNES.

## 1 **References**

- 2 Ackermann, J.: The extinction-to-backscatter ratio of tropospheric aerosol: A numerical  
3 study, *J. Atmos. Ocean. Technol.*, 15, 1043-1050, doi:  
4 10.1175/1520-0426(1998)015<1043:TETBRO>2.0.CO;2, 1998.
- 5 Amiridis, V., Balis, D. S., Giannakaki, E., Stohl, A., Kazadzis, S., Koukouli, M. E. and Zanis,  
6 P.: Optical characteristics of biomass burning aerosols over Southeastern Europe  
7 determined from UV-Raman lidar measurements, *Atmos. Chem. and Phys.*, 9, 2431-2440,  
8 doi:10.5194/acp-9-2431-2009, 2009.
- 9 Andreae, M. O.: Aerosols before Pollution, *Science*, 315, 50-51, 10.2307/20035138, 2007.
- 10 Anguelova, M., Barber Jr, R. P. and Wu, J.: Spume drops produced by the wind tearing of  
11 wave crests, *J. Phys. Oceanogr.*, 29, 1156-1165,  
12 doi:10.1175/1520-0485(1999)029<1156:0.CO;2>, 1999.
- 13 Ansmann, A., Riebesell, M. and Weitkamp, C.: Measurement of atmospheric aerosol  
14 extinction profiles with a Raman lidar, *Opt. Lett.*, 15, 746-748,  
15 doi:10.1364/OL.15.000746, 1990.
- 16 Ansmann, A., Wagner, F., Althausen, D., Müller, D., Herber, A. and Wandinger, U.:  
17 European pollution outbreaks during ACE 2: Lofted aerosol plumes observed with Raman  
18 lidar at the Portuguese coast, *J. Geophys. Res.*, 106, 20725-20,733,  
19 doi:10.1029/2000JD000091, 2001.
- 20 Ansmann, A. and Müller, D.: Lidar and Atmospheric Aerosol Particles, in: Lidar, Weitkamp,  
21 C. (Ed.), Springer New York, 105-141, 2005.
- 22 Bentamy, A., Katsaros, K. B., Mestas-Nuñez, A. M., Drennan, W. M., Forde, E. B. and  
23 Roquet, H.: Satellite estimates of wind speed and latent heat flux over the global oceans, *J.*  
24 *Clim.*, 16, 637-656, doi:10.1175/1520-0442(2003)016<0637:SEOWSA>2.0.CO;2, 2003.
- 25 Blanchard, D. and Woodcock, A.: Bubble formation and modification in the sea and its  
26 meteorological significance, *Tellus*, 9, 145-158, doi: 10.1111/j.2153-3490.1957.tb01867.x,  
27 1957.
- 28 Bloom, S., Da Silva, A., Dee, D., Bosilovich, M., Chern, J., Pawson, S., Schubert, S.,  
29 Sienkiewicz, M., Stajner, I. and Tan, W.: Documentation and validation of the Goddard  
30 Earth Observing System (GEOS) data assimilation system—Version 4, NASA Tech.  
31 Memo., 104606, 187, 2005.
- 32 Blot, R., Clarke, A. D., Freitag, S., Kapustin, V., Howell, S. G., Jensen, J. B., Shank, L. M.,  
33 McNaughton, C. S. and Brekhovskikh, V.: Ultrafine sea spray aerosol over the  
34 southeastern Pacific: open-ocean contributions to marine boundary layer CCN, *Atmos.*  
35 *Chem. Phys.*, 13, 7263-7278, doi:10.5194/acp-13-7263-2013, 2013.

- 1 Bréon, F. M.: Aerosol extinction-to-backscatter ratio derived from passive satellite  
2 measurements, *Atmos. Chem. Phys.*, 13, 8947-8954, doi:10.5194/acp-13-8947-2013,  
3 2013.
- 4 Burton, S., Ferrare, R., Hostetler, C., Hair, J., Rogers, R., Obland, M., Butler, C., Cook, A.,  
5 Harper, D. and Froyd, K.: Aerosol classification using airborne High Spectral Resolution  
6 Lidar measurements—methodology and examples, *Atmos. Meas. Tech.*, 5, 73-98,  
7 doi:10.5194/amtd-4-5631-2011, 2012.
- 8 Burton, S. P., Ferrare, R. A., Vaughan, M. A., Omar, A. H., Rogers, R. R., Hostetler, C. A.,  
9 and Hair, J. W.: Aerosol classification from airborne HSRL and comparisons with the  
10 CALIPSO vertical feature mask, *Atmos. Meas. Tech.*, 6, 1397-1412,  
11 doi:10.5194/amt-6-1397-2013, 2013.
- 12 Carslaw, K. S., Lee, L. A., Reddington, C. L., Pringle, K. J., Rap, A., Forster, P. M., Mann,  
13 G. W., Spracklen, D. V., Woodhouse, M. T., Regayre, L. A. and Pierce, J. R.: Large  
14 contribution of natural aerosols to uncertainty in indirect forcing, *Nature*, 503, 67,  
15 doi:10.1038/nature12674.
- 16 Cattrall, C., Reagan, J., Thome, K. and Dubovik, O.: Variability of aerosol and spectral lidar  
17 and backscatter and extinction ratios of key aerosol types derived from selected Aerosol  
18 Robotic Network locations, *J. Geophys. Res.*, 110, D10S11, doi:10.1029/2004JD005124,  
19 2005.
- 20 de Leeuw, G., Andreas, E. L., Anguelova, M. D., Fairall, C., Lewis, E. R., O'Dowd, C.,  
21 Schulz, M. and Schwartz, S. E.: Production flux of sea spray aerosol, *Rev. Geophys.*, 49,  
22 doi:10.1029/2010RG000349, 2011.
- 23 Doherty, S. J., Anderson, T. L. and Charlson, R. J.: Measurement of the lidar ratio for  
24 atmospheric aerosols with a 180 backscatter nephelometer, *Appl. Opt.*, 38, 1823-1832,  
25 1999.
- 26 Eloranta, E.: High spectral resolution lidar, in: *Lidar: Range-Resolved Optical Remote  
27 Sensing of the Atmosphere*, edited by: Weitkamp, K., Springer, New York, 143-163,  
28 2005.
- 29 Fernald, F. G., Herman, B. M. and Reagan, J. A.: Determination of aerosol height  
30 distributions by lidar, *J. Appl. Meteorol.*, 11, 482-489, 1972.
- 31 Fuentes, E., Coe, H., Green, D. and McFiggans, G.: On the impacts of phytoplankton-derived  
32 organic matter on the properties of the primary marine aerosol - Part 2: Composition,  
33 hygroscopicity and cloud condensation activity, *Atmos. Chem. Phys.*, 11, 2585-2602,  
34 doi:10.5194/acp-11-2585-2011, 2011.
- 35 Ghan, S., Laulainen, N., Easter, R., Wagener, R., Nemesure, S., Chapman, E., Zhang, Y. and  
36 Leung, R.: Evaluation of aerosol direct radiative forcing in MIRAGE, *J. Geophys. Res.*,  
37 106, 5295-5316, doi:10.1029/2000JD900502, 2001.

- 1 Groß S., Esselborn, M., Weinzierl, B., Wirth, M., Fix, A. and Petzold, A.: Aerosol  
2 classification by airborne high spectral resolution lidar observations, *Atmos. Chem. Phys.*,  
3 13, 2487-2505, doi:10.5194/acp-13-2487-2013, 2013.
- 4 Groß, S., Gasteiger, J., Freudenthaler, V., Wiegner, M., Geiß, A., Schladitz, A., Toledano, C.,  
5 Kandler, K., Tesche, M., Ansmann, A. and Wiedensohler, A.: Characterization of the  
6 planetary boundary layer during SAMUM-2 by means of lidar measurements, *Tellus B*,  
7 63, 695-705, doi:10.1111/j.1600-0889.2011.00557.x, 2011a.
- 8 Groß S., Tesche, M., Voker, F., Toledano, C., Wiegner, M., Ansmann, A., Althausen, D.,  
9 Seefeldner, M.: Characterization of Saharan dust, marine aerosols and mixtures of  
10 biomass-burning aerosols and dust by means of multi-wavelength depolarization and  
11 Raman lidar measurements during SAMUM 2, *Tellus B*, 63, 706-724,  
12 doi:10.1111/j.1600-0889.2011.00556.x, 2011b.
- 13 Grund, C. J. and Eloranta, E. W.: University of Wisconsin High Spectral Resolution Lidar,  
14 *Optical Engineering*, 30, 6-12, doi:10.1117/12.55766, 1991.
- 15 Hair, J. W., Hostetler, C. A., Cook, A. L., Harper, D. B., Ferrare, R. A., Mack, T. L., Welch,  
16 W., Izquierdo, L. R. and Hovis, F. E.: Airborne High Spectral Resolution Lidar for  
17 profiling aerosol optical properties, *Appl. Opt.*, 47, 6734-6752,  
18 doi:10.1364/AO.47.006734, 2008.
- 19 Hoffman, E. J. and Duce, R. A.: The organic carbon content of marine aerosols collected on  
20 Bermuda, *J. Geophys. Res.*, 79, 4474-4477, 1974.
- 21 Holben, B. N., Eck, T. F., Slutsker, I., Tanré, D., Buis, J. P., Setzer, A., Vermote, E., Reagan,  
22 J. A., Kaufman, Y. J., Nakajima, T., Lavenu, F., Jankowiak, I. and Smirnov, A.:  
23 AERONET-A Federated Instrument Network and Data Archive for Aerosol  
24 Characterization, *Remote Sens. Environ.*, 66, 1, doi:10.1016/S0034-4257(98)00031-5,  
25 1998.
- 26 Hoose, C., Kristjánsson, J., Iversen, T., Kirkevåg, A., Seland, Ø and Gettelman, A.:  
27 Constraining cloud droplet number concentration in GCMs suppresses the aerosol indirect  
28 effect, *Geophys. Res. Lett.*, 36, L12807, doi:10.1029/2009GL038568, 2009.
- 29 Hostetler, C., Liu, Z., Reagan, J., Vaughan, M., Winker, D., Osborn, M., Hunt, W., Powell,  
30 K. and Trepte, C.: CALIOP algorithm theoretical basis document—Part 1: Lidar level I  
31 ATBD-Calibration and level 1 data products, *Rep.PC-SCI*, 201, 66, 2005.
- 32 Josset, D., Pelon, J., Protat, A. and Flamant, C.: New approach to determine aerosol optical  
33 depth from combined CALIPSO and CloudSat ocean surface echoes, *Geophys. Res. Lett.*,  
34 35, L10805, doi:10.1029/2008GL033442, 2008.
- 35 Josset, D., Pelon, J. and Hu, Y.: Multi-instrument calibration method based on a  
36 multiwavelength ocean surface model, *Geoscience and Remote Sensing Letters, IEEE*, 7,  
37 195-199, doi:10.1109/LGRS.2009.2030906, 2010a.
- 38 Josset, D., Zhai, P., Hu, Y., Pelon, J. and Lucker, P. L.: Lidar equation for ocean surface and  
39 subsurface, *Opt. Express*, 18, 20862-20875, doi:10.1364/OE.18.020862, 2010b.

- 1 Josset, D., Rogers, R., Pelon, J., Hu, Y., Liu, Z., Omar, A. and Zhai, P.: CALIPSO lidar ratio  
2 retrieval over the ocean, *Opt. Express*, 19, 18696-18706, doi:10.1364/OE.19.018696,  
3 2011.
- 4 Josset, D., Pelon, J., Garnier, A., Hu, Y., Vaughan, M., Zhai, P., Kuehn, R. and Lucker, P.:  
5 Cirrus optical depth and lidar ratio retrieval from combined CALIPSO-CloudSat  
6 observations using ocean surface echo, *J. Geophys. Res.*, 117, D05207,  
7 doi:10.1029/2011JD016959, 2012.
- 8 Kaufman, Y. J., Tanré, D. and Boucher, O.: A satellite view of aerosols in the climate system,  
9 *Nature*, 419, 215-223, doi:10.1038/nature01091, 2002.
- 10 Kiliyanpilakkil, V. P. and Meskhidze, N.: Deriving the effect of wind speed on clean marine  
11 aerosol optical properties using the A-Train satellites, *Atmos. Chem. Phys.*, 11,  
12 11401-11413, doi:10.5194/acp-11-11401-2011, 2011.
- 13 Kleidman, R.G., Smirnov, A., Levy, R.C., Mattoo, S., Tanre, D.: Evaluation and Wind Speed  
14 Dependence of MODIS Aerosol Retrievals Over Open Ocean, *IEEE T Geosci Remote*,  
15 vol.50, no.2, pp.429,435, Feb. 2012, doi:10.1109/TGRS.2011.2162073, 2010.
- 16 Lehahn, Y., Koren, I., Boss, E., Ben-Ami, Y. and Altaratz, O.: Estimating the maritime  
17 component of aerosol optical depth and its dependency on surface wind speed using  
18 satellite data, *Atmos. Chem. Phys.*, 10, 6711-6720, doi:10.5194/acp-10-6711-2010, 2010.
- 19 Levy, R., Remer, L., Martins, J., Kaufman, Y., Plana-Fattori, A., Redemann, J. and Wenny,  
20 B.: Evaluation of the MODIS aerosol retrievals over ocean and land during CLAMS, *J.*  
21 *Atmos. Sci.*, 62, 974-992, doi:10.1175/JAS3391.1, 2005.
- 22 Lewis, R. and Schwartz, E.: Sea salt aerosol production: mechanisms, methods,  
23 measurements and models—a critical review, American Geophysical Union,  
24 doi:10.1029/GM152, 2004.
- 25 Masonis, S. J., Anderson, T. L., Covert, D. S., Kapustin, V., Clarke, A. D., Howell, S. and  
26 Moore, K.: A Study of the Extinction-to-Backscatter Ratio of Marine Aerosol during the  
27 Shoreline Environment Aerosol Study, *J. Atmos. Ocean. Technol.*, 20, 1388-1402,  
28 doi:10.1175/1520-0426(2003)020<1388:ASOTER>2.0.CO;2, 2003.
- 29 Meskhidze, N., Xu, J., Gantt, B., Zhang, Y., Nenes, A., Ghan, S., Liu, X., Easter, R. and  
30 Zaveri, R.: Global distribution and climate forcing of marine organic aerosol—Part 1:  
31 Model improvements and evaluation, *Atmos. Chem. Phys.*, 11, 11689-11705,  
32 doi:10.5194/acp-11-11689-2011, 2011.
- 33 Müller, D., Ansmann, A., Mattis, I., Tesche, M., Wandinger, U., Althausen, D. and Pisani,  
34 G.: Aerosol-type-dependent lidar ratios observed with Raman lidar, *J. Geophys. Res.*, 112,  
35 10.1029/2006JD008292, 2007.
- 36 Omar, A. H., Winker, D. M., Kittaka, C., Vaughan, M. A., Liu, Z., Hu, Y., Trepte, C. R.,  
37 Rogers, R. R., Ferrare, R. A., Lee, K., Kuehn, R. E. and Hostetler, C. A.: The CALIPSO  
38 Automated Aerosol Classification and Lidar Ratio Selection Algorithm, *J. Atmos. Ocean.*  
39 *Technol.*, 26, 1994-2014, doi:10.1175/2009JTECHA1231.1, 2009.

- 1 Oo, M. and Holz, R.: Improving the CALIOP aerosol optical depth using combined MODIS-  
2 CALIOP observations and CALIOP integrated attenuated total color ratio, *J. Geophys.*  
3 *Res.*, 116, D14201, doi:10.1029/2010JD014894, 2011.
- 4 Ovadnevaite, J., Ceburnis, D., Martucci, G., Bialek, J., Monahan, C., Rinaldi, M., Facchini,  
5 M. C., Berresheim, H., Worsnop, D. R. and O'Dowd, C.: Primary marine organic aerosol:  
6 A dichotomy of low hygroscopicity and high CCN activity, *Geophys. Res. Lett.*, 38,  
7 doi:10.1029/2011GL048869, 2011.
- 8 Piironen, P. and Eloranta, E.: Demonstration of a high-spectral-resolution lidar based on an  
9 iodine absorption filter, *Opt. Lett.*, 19, 234-236, 1994.
- 10 Redemann, J., Vaughan, M. A., Zhang, Q., Shinozuka, Y., Russell, P. B., Livingston, J. M.,  
11 Kacenelenbogen, M., and Remer, L. A.: The comparison of MODIS-Aqua (C5) and  
12 CALIOP (V2 & V3) aerosol optical depth, *Atmos. Chem. Phys.*, 12, 3025-3043,  
13 doi:10.5194/acp-12-3025-2012, 2012.
- 14 Saxena, P., Hildemann, L. M., McMurry, P. H. and Seinfeld, J. H.: Organics alter  
15 hygroscopic behavior of atmospheric particles, *J. Geophys. Res.*, 100, 18755-18770,  
16 doi:10.1029/95JD01835, 1995.
- 17 Sayer, A., Smirnov, A., Hsu, N. and Holben, B.: A pure marine aerosol model, for use in  
18 remote sensing applications, *J. Geophys. Res.*, 117, doi:10.1029/2011JD016689, 2012.
- 19 Schuster, G. L., Vaughan, M., MacDonnell, D., Su, W., Winker, D., Dubovik, O., Lapyonok,  
20 T. and Trepte, C.: Comparison of CALIPSO aerosol optical depth retrievals to AERONET  
21 measurements, and a climatology for the lidar ratio of dust, *Atmos. Chem. Phys.*, 12,  
22 7431-7452, doi:10.5194/acp-12-7431-2012, 2012
- 23 Shipley, S. T., Tracy, D., Eloranta, E. W., Trauger, J. T., Sroga, J., Roesler, F. and Weinman,  
24 J. A.: High spectral resolution lidar to measure optical scattering properties of atmospheric  
25 aerosols. 1: Theory and instrumentation, *Appl. Opt.*, 22, 3716-3724, 1983.
- 26 Smirnov, A., Holben, B., Eck, T., Dubovik, O. and Slutsker, I.: Effect of wind speed on  
27 columnar aerosol optical properties at Midway Island, *J. Geophys. Res.*, 108(D24), 4802,  
28 doi:10.1029/2003JD003879, 2003.
- 29 Smirnov, A., Holben, B. N., Giles, D. M., Slutsker, I., O'Neill, N. T., Eck, T. F., Macke, A.,  
30 Croot, P., Courcoux, Y., Sakerin, S. M., Smyth, T. J., Zielinski, T., Zibordi, G., Goes, J. I.,  
31 Harvey, M. J., Quinn, P. K., Nelson, N. B., Radionov, V. F., Duarte, C. M., Losno, R.,  
32 Sciare, J., Voss, K. J., Kinne, S., Nalli, N. R., Joseph, E., Krishna Moorthy, K.,  
33 Covert, D. S., Gulev, S. K., Milinevsky, G., Larouche, P., Belanger, S., Horne, E.,  
34 Chin, M., Remer, L. A., Kahn, R. A., Reid, J. S., Schulz, M., Heald, C. L., Zhang, J.,  
35 Lapina, K., Kleidman, R. G., Griesfeller, J., Gaitley, B. J., Tan, Q., and Diehl, T. L.:  
36 Maritime aerosol network as a component of AERONET – first results and comparison  
37 with global aerosol models and satellite retrievals, *Atmos. Meas. Tech.*, 4, 583-597,  
38 doi:10.5194/amt-4-583-2011, 2011.
- 39 Smirnov, A., Holben, B. N., Slutsker, I., Giles, D. M., McClain, C. R., Eck, T. F., Sakerin, S.  
40 M., Macke, A., Croot, P., Zibordi, G., Quinn P. K., Sciare, J., Kinne, S., Harvey, M.,

- 1 Smyth, T. J., Piketh S., Zielinski, T., Proshutinsky A., Goes, J. I., Nelson, N. B., Larouche,  
2 P., Radionov, V. F., Goloub, P., Krishna Moorthy, K., Matarrese, R., Robertson, E. J. and  
3 Jourdin, F.: Maritime Aerosol Network as a component of Aerosol Robotic Network, *J.*  
4 *Geophys. Res.*, 114, D06204, doi:10.1029/2008JD011257, 2009.
- 5 Tesche, M., Ansmann, A., Müller, D., Althausen, D., Engelmann, R., Freudenthaler, V. and  
6 Groß, S.: Vertically resolved separation of dust and smoke over Cape Verde using  
7 multiwavelength Raman and polarization lidars during Saharan Mineral Dust Experiment  
8 2008, *J. Geophys. Res.*, 114, n/a-n/a, doi:10.1029/2009JD011862, 2009a.
- 9 Tesche, M., Ansmann, A., Müller, D., Althausen, D., Mattis, I., Heese, B., Freudenthaler, V.,  
10 Wiegner, M., Esselborn, M., Pisani, G., and Knippertz, P.: Vertical profiling of Saharan  
11 dust with Raman lidars and airborne HSRL in southern Morocco during SAMUM, *Tellus*  
12 *B*, 61, 144-164, doi:10.1111/j.1600-0889.2008.00390.x, 2009b.
- 13 Vaughan, M. A., Young, S. A., Winker, D. M., Powell, K. A., Omar, A. H., Liu, Z., Hu, Y.  
14 and Hostetler, C. A.: Fully automated analysis of space-based lidar data: An overview of  
15 the CALIPSO retrieval algorithms and data products, *Proc. SPIE 5575, Laser Radar*  
16 *Techniques for Atmospheric Sensing*, 16, doi:10.1117/12.572024, 2004.
- 17 Vaughan, M. A., Powell, K. A., Kuehn, R. E., Young, S. A., Winker, D. M., Hostetler, C. A.,  
18 Hunt, W. H., Liu Z., McGill, M. J. and Getzewich, B. J.: Fully automated detection of  
19 cloud and aerosol layers in the CALIPSO lidar measurements, *J. Atmos. Ocean Technol.*,  
20 26, 2034-2050, doi:10.1175/2009JTECHA1228.1, 2009.
- 21 Wang, M. and Penner, J.: Aerosol indirect forcing in a global model with particle nucleation,  
22 *Atmos. Chem. Phys.*, 9, 239-260, doi:10.5194/acp-9-239-2009, 2009.
- 23 Westervelt, D., Moore, R., Nenes, A. and Adams, P.: Effect of primary organic sea spray  
24 emissions on cloud condensation nuclei concentrations, *Atmos. Chem. Phys.*, 12, 89-101,  
25 doi:10.5194/acp-12-89-2012, 2012.
- 26 Winker, D. M., Vaughan, M. A., Omar, A., Hu, Y., Powell, K. A., Liu, Z., Hunt, W. H. and  
27 Young, S. A.: Overview of the CALIPSO mission and CALIOP data processing  
28 algorithms, *J. Atmos. Ocean. Technol.*, 26, 2310-2323, doi:10.1175/2009JTECHA1281.1  
29 2009.
- 30 Young, S. A., Cutten, D. R., Lynch, M. J. and Davies, J. E.: Lidar-derived variations in the  
31 backscatter-to-extinction ratio in southern hemisphere coastal maritime aerosols, *Atmos.*  
32 *Environ.*, 27, 1541-1551, doi:10.1016/0960-1686(93)90154-Q, 1993.
- 33 Young, S. A. and Vaughan, M. A.: The retrieval of profiles of particulate extinction from  
34 cloud-aerosol lidar infrared pathfinder satellite observations (CALIPSO) data: algorithm  
35 description, *J. Atmos. Oceanic Technol.*, 26, 1105-1119,  
36 doi:10.1175/2008JTECHA1221.1, 2009.

37

38



1 **Tables**

2

3 **Table 1.** Seasonal means  $\pm$  1 standard deviations for  $2^\circ \times 5^\circ$  grid cell medians. The  
 4 subscripts p, S, and C appended to  $\tau$  stand for particulate, SODA, and CALIOP,  
 5 respectively, where  $\tau$  is the AOD.  
 6  
 7

Season	SODA $\tau_{p,S}$	CALIOP $\tau_{p,C}$	$\Gamma_p, \times 10^{-3}$ sr <sup>-1</sup>	$S_p$ sr
Winter	0.14 $\pm$ 0.04	0.09 $\pm$ 0.03	4.7 $\pm$ 1.2	27 $\pm$ 8
Spring	0.13 $\pm$ 0.03	0.09 $\pm$ 0.03	4.8 $\pm$ 1.2	24 $\pm$ 7
Summer	0.14 $\pm$ 0.04	0.09 $\pm$ 0.03	4.6 $\pm$ 1.2	27 $\pm$ 8
Fall	0.13 $\pm$ 0.03	0.09 $\pm$ 0.03	4.7 $\pm$ 1.1	25 $\pm$ 7

8

9

1 **Table 2.** Means  $\pm$  1 standard deviation for  $2^\circ \times 5^\circ$  grid cell medians for various AMSR-E  
2 wind speed regimes. The subscripts S and C appended to  $\tau$  stand for SODA and CALIOP,  
3 respectively, where  $\tau$  is the AOD.  
4

Wind Regime $\text{ms}^{-1}$	SODA $\tau_S$	CALIOP $\tau_C$	$\Gamma_p, \times 10^{-3}$ $\text{sr}^{-1}$	$S_p$ sr	Number absolute(%)
$0 < U_{10} \leq 4$	0.12 $\pm$ 0.05	0.07 $\pm$ 0.04	3.6 $\pm$ 1.4	32 $\pm$ 17	11849 (5)
$4 < U_{10} \leq 6$	0.11 $\pm$ 0.04	0.07 $\pm$ 0.03	3.8 $\pm$ 1.1	27 $\pm$ 12	32899 (13)
$6 < U_{10} \leq 8$	0.12 $\pm$ 0.04	0.08 $\pm$ 0.02	4.2 $\pm$ 1.0	26 $\pm$ 9	60083 (23)
$8 < U_{10} \leq 10$	0.13 $\pm$ 0.03	0.08 $\pm$ 0.02	4.7 $\pm$ 1.0	26 $\pm$ 7	68899 (26)
$10 < U_{10} \leq 12$	0.15 $\pm$ 0.04	0.10 $\pm$ 0.03	5.1 $\pm$ 1.0	26 $\pm$ 6	45895 (17)
$12 < U_{10} \leq 15$	0.16 $\pm$ 0.04	0.12 $\pm$ 0.03	5.7 $\pm$ 1.2	25 $\pm$ 6	30162 (11)
$U_{10} > 15$	0.16 $\pm$ 0.04	0.14 $\pm$ 0.04	6.4 $\pm$ 1.4	22 $\pm$ 7	12953 (5)

# 1 Figures

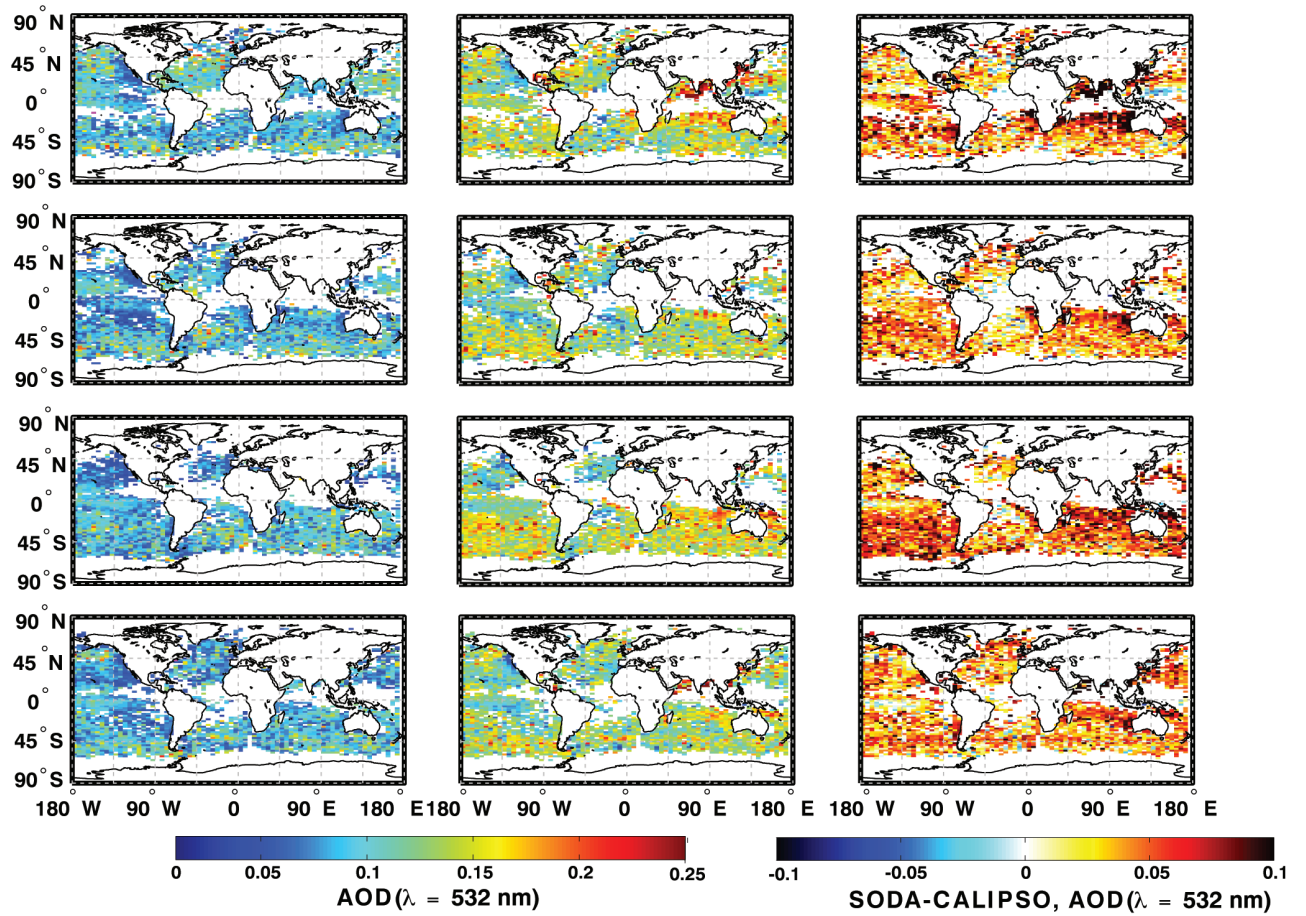
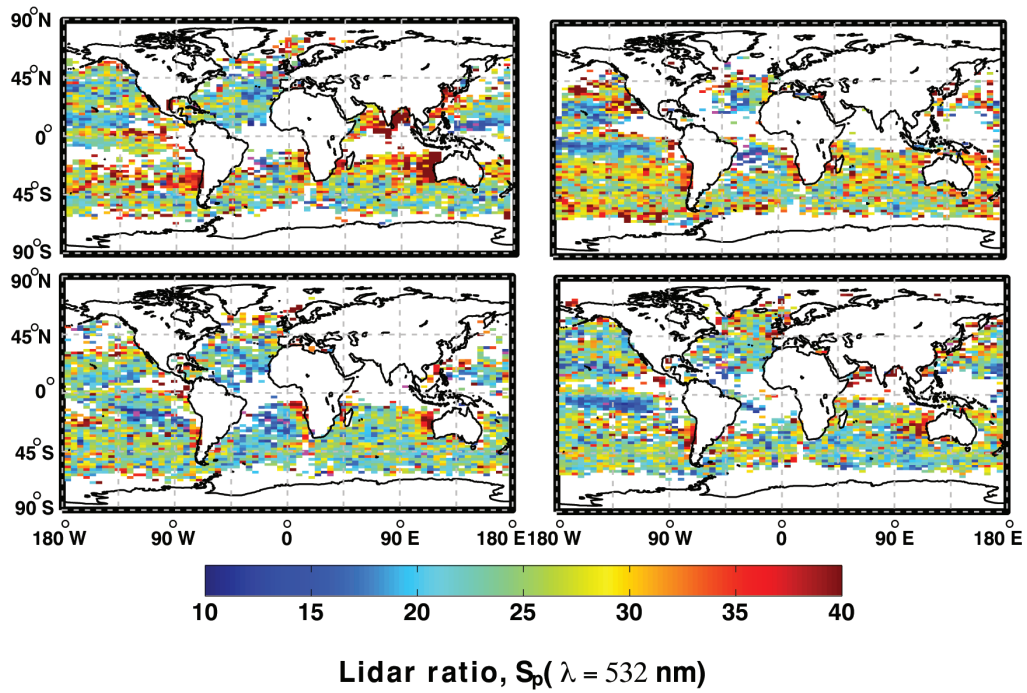


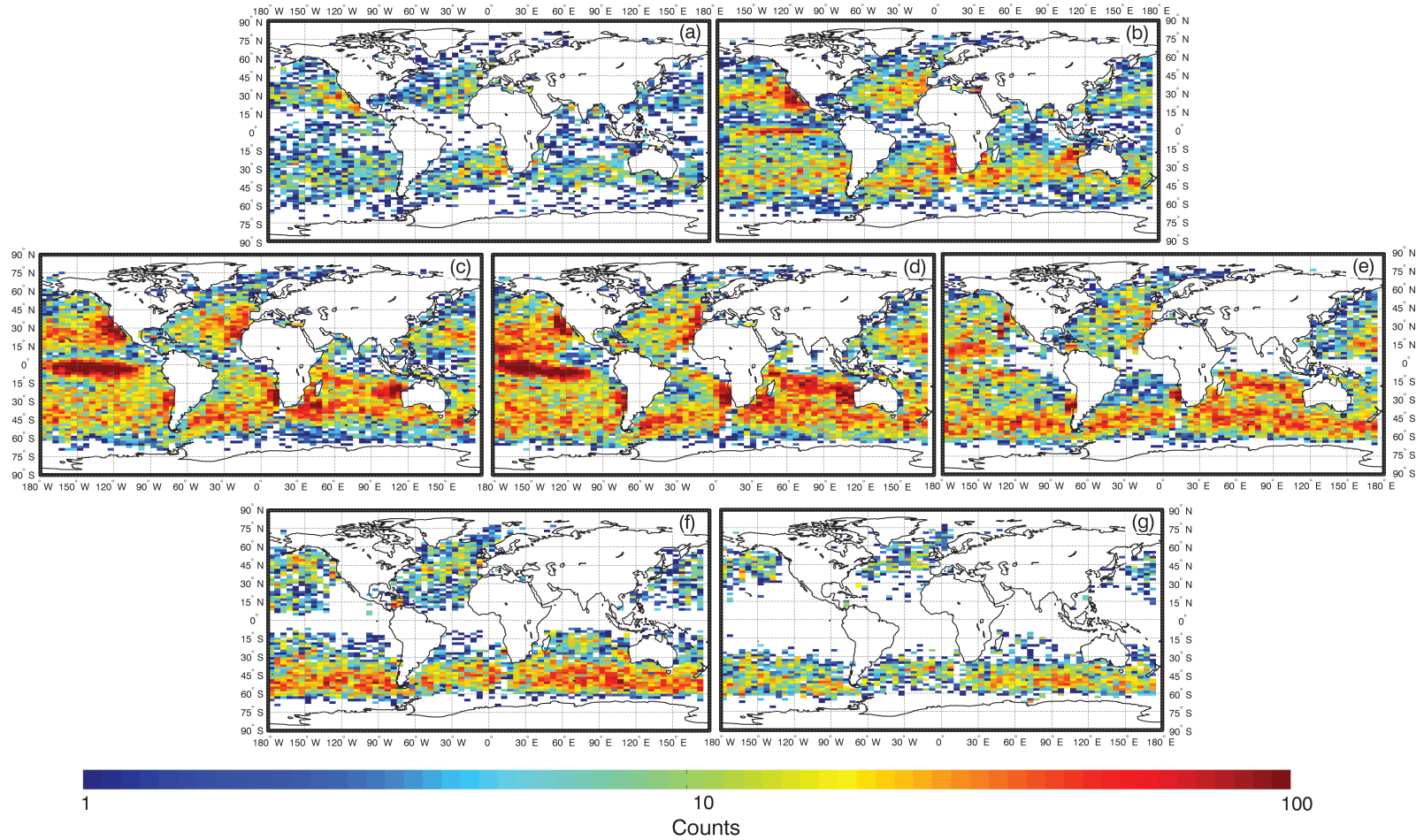
**Fig. 1** - Seasonal median AOD values from CALIOP and SODA (columns 1 and 2) and the difference (SODA – CALIOP) plot (column 3) for December - February (row 1), March - May (row 2), June - August (row 3), September - November (row 4) plotted on a  $2^\circ \times 5^\circ$  latitude longitude grid. “No Data” is shaded white and is defined as grid cells failing quality control algorithm (see text for details).



1

2 **Fig. 2** - Seasonal lidar ratio for  $2^\circ \times 5^\circ$  latitude longitude grid cells. Seasons are arranged as  
 3 (a) December - February , (b) March - May, (c) June - August, (d) September - November.

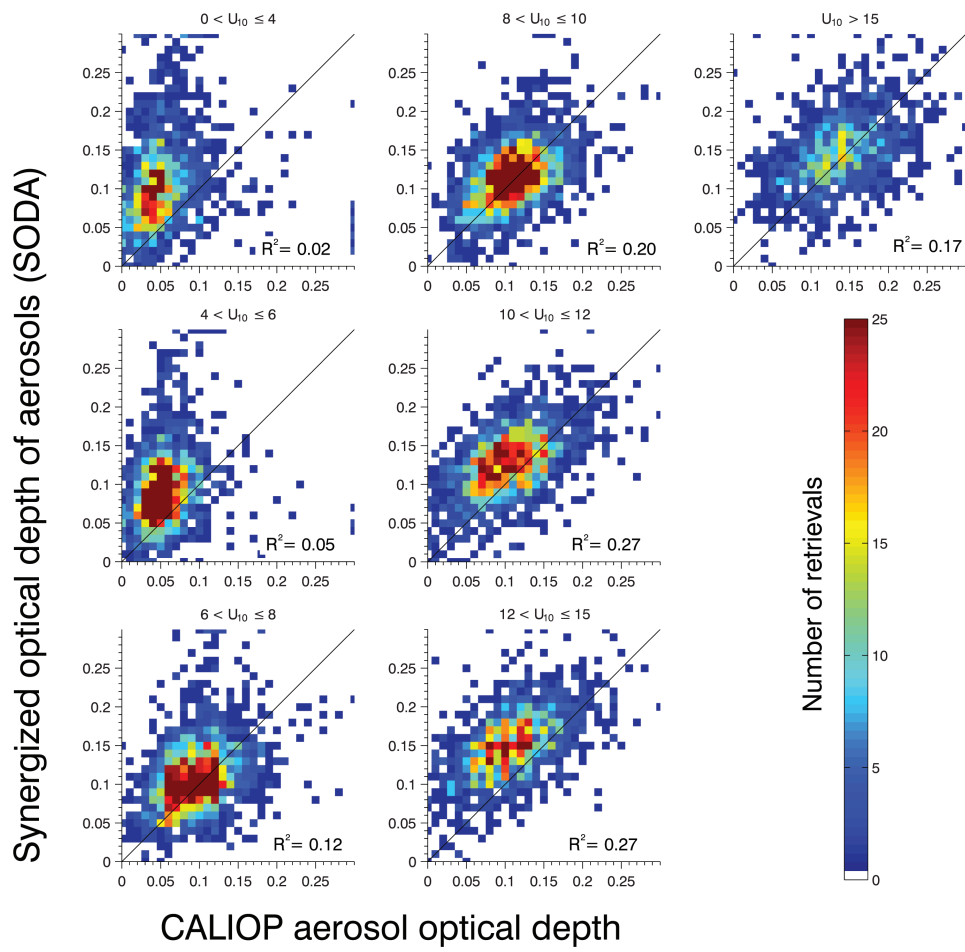
1



2  
3

4 **Fig. 3** - SODA/CALIOP retrieval counts for each  $2^\circ \times 5^\circ$  latitude longitude grid cell and different wind speed regimes. AMSR-E wind speed  
5 regimes for figures (a) through (g), are 0-4, 4-6, 6-8, 8-10, 10-12, 12-15, and  $>15 \text{ m s}^{-1}$ , respectively.

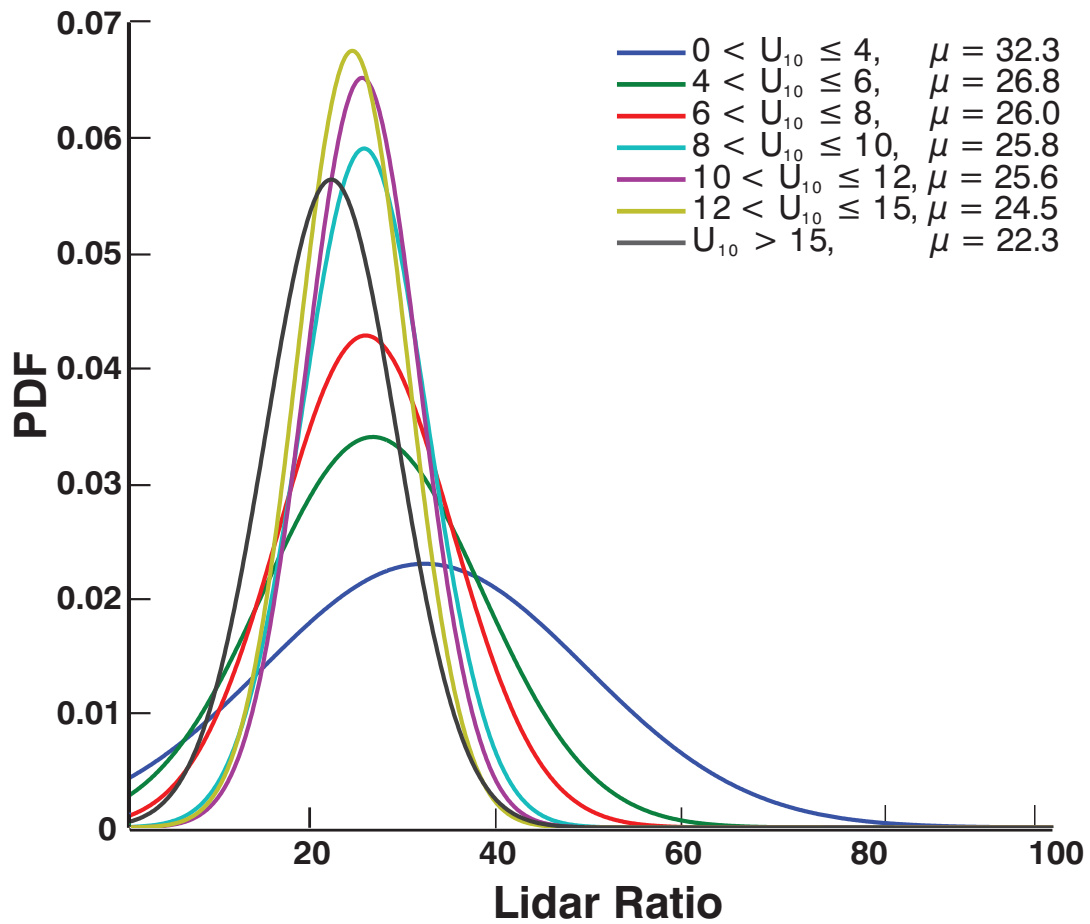
1



2

3 **Fig. 4** - Scatter density plot of SODA to CALIOP AOD for each wind speed regime. Each  
4 point indicates a grid cell median, colored by frequency of occurrence. The black line is the  
5 1:1 relationship, with reported  $R^2$  values.

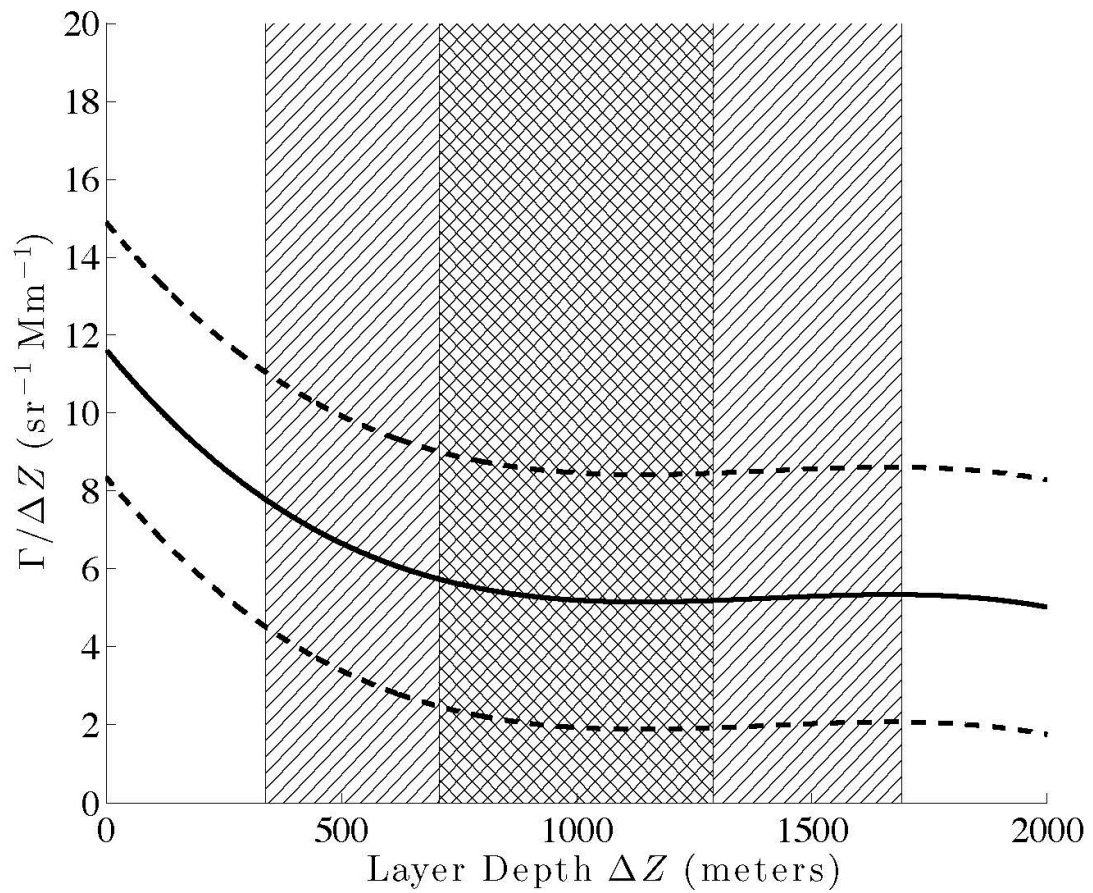
6



1

2 **Fig. 5** - Probability density function of clean marine aerosol lidar ratio for selected AMSR-E  
 3 wind speed regimes. The mean ( $\mu$ ) of each distribution is also reported.

4

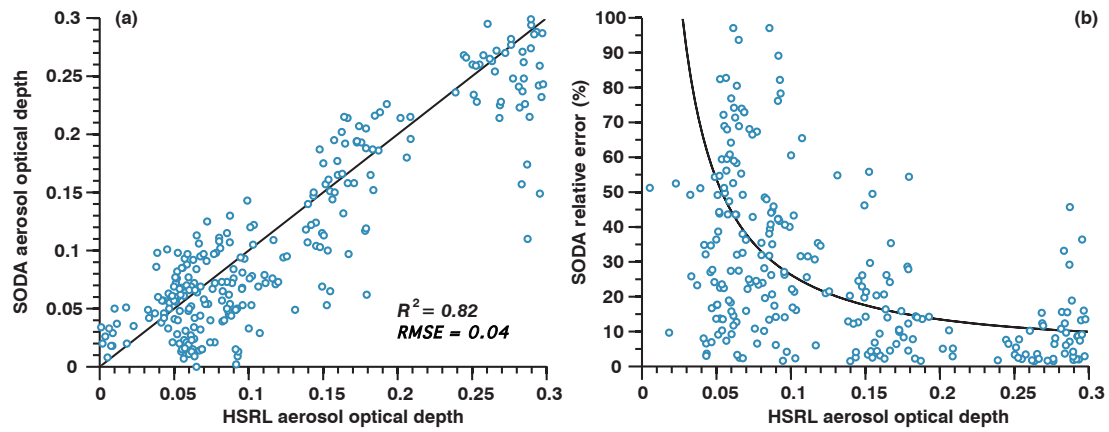


1

2 **Fig. 6** - The normalised integrated attenuated backscatter as a function of the layer depth. The  
 3 solid line shows the 3<sup>rd</sup> order least squares fit to the data while the dotted lines show  $\pm 1\sigma$ ; the  
 4 hatched area shows the layer depth data frequency: cross hatch between the 25<sup>th</sup> and 75<sup>th</sup>  
 5 percentiles and straight hatch between 5<sup>th</sup> and 95<sup>th</sup> percentiles.

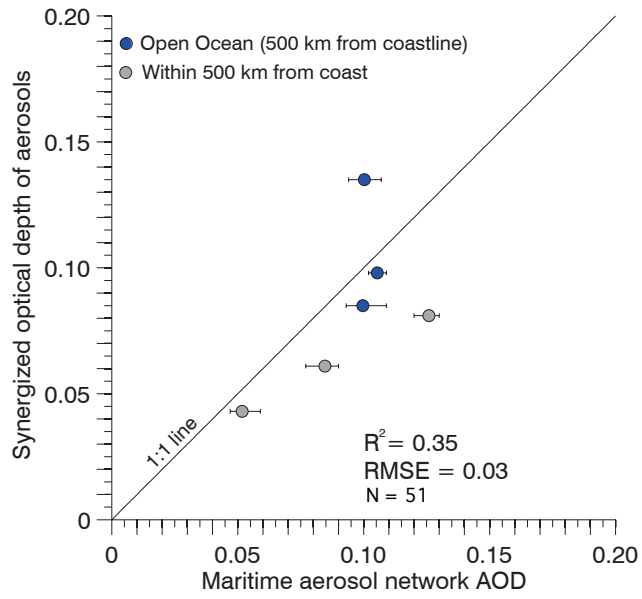
6





1  
2  
3  
4  
5  
6  
7  
8

**Fig. 7** - (a) A scatter plot of SODA AOD relative to AOD measured by HSRL at 532 nm with corresponding  $R^2$  and RMSE. The black line illustrates the 1:1 line. (b) Relative uncertainty in the SODA column lidar ratio as a function of HSRL AOD with the black line showing the least squares exponential fit as in Josset et al. (2012), Eq. 15. All points are classified as marine plus pollution or marine plus dust and are from Table 1 in Josset et al. (2011).



1

2 **Fig. 8** – Scatter plot comparing the aerosol optical depth from SODA (y-axis) and  
 3 AERONET maritime aerosol network (MAN; x-axis). Blue circles represent locations that  
 4 are at least 500 km from a coastline and are considered to be “open ocean”.